HHS Public Access

Author manuscript

J Am Chem Soc. Author manuscript; available in PMC 2019 August 08.

Published in final edited form as:

J Am Chem Soc. 2018 August 08; 140(31): 9793–9796. doi:10.1021/jacs.8b04319.

Engineering a 3D DNA-Logic Gate Nanomachine for Bispecific Recognition and Computing on Target Cell Surfaces

Ruizi Peng[†,#], **Xiaofang Zheng**[†,#], **Yifan Lyu**[†,‡,§], **Liujun Xu**[†], **Xiaobing Zhang**[†], **Guoliang Ke**[†], **Qiaoling Liu**[†], **Changjun You**[†], **Shuangyan Huan**[*,†], and **Weihong Tan**[*,†,‡,§]

[†]Molecular Science and Biomedicine Laboratory (MBL), State Key Laboratory of Chemo/Bio-Sensing and Chemometrics, College of Chemistry and Chemical Engineering, College of Life Sciences, Aptamer Engineering Center of Hunan Province, Hunan University, Changsha 410082, People's Republic of China

[‡]Institute of Molecular Medicine, Renji Hospital, Shanghai Jiao Tong University School of Medicine, and College of Chemistry and Chemical Engineering, Shanghai Jiao Tong University, Shanghai 200240, People's Republic of China

[§]Department of Chemistry and Physiology and Functional Genomics, Center for Research at the Bio/Nano Interface, Health Cancer Center, UF Genetics Institute, McKnight Brain Institute, University of Florida, Gainesville, Florida 32611-7200, United States

Abstract

Among the vast number of recognition molecules, DNA aptamers generated from cell-SELEX exhibit unique properties for identifying cell membrane biomarkers, in particular protein receptors on cancer cells. To integrate all recognition and computing modules within a single structure, a three-dimensional (3D) DNA-based logic gate nanomachine was constructed to target overexpressed cancer cell biomarkers with bispecific recognition. Thus, when the Boolean operator "AND" returns a true value, it is followed by an "ON" signal when the specific cell type is presented. Compared with freely dispersed double-stranded DNA (dsDNA)-based molecular circuits, this 3D DNA nanostructure, termed DNA-logic gate triangular prism (TP), showed better identification performance, enabling, in turn, better molecular targeting and fabrication of recognition nanorobotics.

Within the boundary of the cell membrane surface are found thousands of components, all of which play essential biological roles in cell−cell communication, cell growth, proliferation and death.[1] Many of these components consist of protein receptors, often overexpressed, which can be a rich source of biomarker discovery for disease diagnosis, therapeutics and biomedical engineering.[2] However, the priorities are molecular recognition of these overexpressed objects and production of a computational signal, so that final actuation can be achieved for biomedical applications. Therefore, the use of a Boolean logic-based molecular system to sort and identify these biomarkers has garnered substantial attention

[*]**Corresponding Authors** tan@chem.ufl.edu, shuangyanhuan@163.com.
[#]These authors contributed equally to this work.

Notes

The authors declare no competing financial interest.

over the past few years. Nanomachines were recently created to process molecular signals on cell surface.[3] The fundamental element of these nanomachines involves target recognition. Accordingly, harnessing the affinity of antibodies and aptamers toward their target membrane receptors, the relative concentrations and affinities of these moieties were analyzed to determine a particular cell type,[4] leading to many logic-based molecular machines built for biomedical applications.[5] However, typical logic gate nanomachines consist of several freely diffusible components in solution, thus severely lowering the logic operation speed for molecular proximity effect.[6]

To address this issue, nanomachines were fabricated by logic operation components in a constrained platform, including nanoparticles,[7] organic scaffolds[8] and DNA assemblies.[9] The unique properties enable DNA nanoarchitectures[10] to play dynamic operations;[11] consequently, engineered by elements integration strategy, DNA aptamer-based nanomachines became the smart systems of choice for logic gate computation on the cell surface.[12] DNA aptamers generated from cell-SELEX (Systematic Evolution of Ligands by EXponential enrichment) exhibit both high specificity and high binding affinity, and they can be easily synthesized and chemically modified.[13] Importantly, because aptamers are oligonucleotides, they can be displaced by DNA strands. On the basis of our previous study[14] and considering the dimensional factor for 3D structures showing the superior stability[15] and cellular internalization ability,[16] we herein engineered a small DNA-logic gate triangular prism (TP) as a 3D DNA nanomachine for cell-surface recognition and computing (Figure 1).

In order to construct a 3D DNA nanostructure model, a DNA TP was initially designed for subsequent functionalization that meets the minimal-use requirements for DNA strands[17] (Figures S1 and S2). Its top face and two side faces extend functional toes. Bispecific recognition is used to overcome heterogeneity among cancer cell subtypes,[18] as revealed by individual markers on the target cell surface. On the top face, a reporter toe, consisting of the conjugates of strands F, S and R (F/S/R), was loaded, while two separate recognition toes (sgc8c/cS and sgc4f/cF) were loaded on the bottom face (Figure 1a).

To perform the “AND” Boolean logic operation for the target cell surface, two aptamers, sgc8c (targeting tyrosine-protein kinase-like 7) and sgc4f (unidentified target), were selected to serve as recognition molecules to target overexpressed cancer biomarkers in human acute lymphoblastic leukemia cells (CCRF-CEM), but neither in Ramos cells, making it possible to identify these two cell types based on aptamer recognition.[13a,14] In the absence of CEM cells, each aptamer hybridizes with a piece of its respective complementary DNA (cDNA). However, in the presence of CEM cells expressing both target biomarkers, this aptamer/cDNA conjugate switches to an aptamer/target conjugate, while releasing cDNA as an output. As shown in Figure 1b, when two kinds of outputs are released from the recognition toes, the reporter toe is turned on after undergoing DNA strand displacement reactions. While target recognition is important, signal response depends on the strength of expression, and, in this case, because both biomarkers are underexpressed on the Ramos cell membrane, insufficient signal response precludes the execution of computing operations.

Initially, a 3D DNA TP was one-pot self-assembled (Figures S3 and S4). As each edge of the equilateral triangle has a single strand domain for hybridizing functional toes (Figure 2a), a functional toes loaded DNA nanomachine was created. Native polyacrylamide gel electrophoresis (native-PAGE) was used to verify the functional transformation from this TP scaffold to DNA nanomachine (Figure 2b), in agreement with the result of size change by dynamic light scattering (DLS, Figures 2c and S5). Then, the feasibility of "AND" logic operation was initially investigated using complementary DNA strands instead of cell surface biomarkers. The "ON" reporter signal for recovery of fluorescence on the R strand was observed only if stimulated by complete complementarity to strand S and a piece of sgc8c (cS), as well as complete complementarity to strand F and a piece of sgc4f (cF); otherwise, the reporter is "OFF" (Figure 1b). To verify this dual-input process, different fluorescence ratio groups of cS and cF were studied on a reporter toe-loaded DNA TP (F/S/R-TP). Little difference for fluorescence recovery between different ratio groups of cS strand indicated equal cS to cF can make this logic operations efficient (Figure 2f). Finally, when both target strands existed, the "ON" response occurred (Figure 2g), in agreement with the native-PAGE result (Figure 2e).

Different from double stranded DNA (dsDNA) systems, which normally make up DNA molecular circuits, 3D nanostructures are more stable and more easily uptaken by cells.[16] Hence, fluorophores labeled dsDNA (sgc8c/cS) was created, and flow cytometry was employed to analyze the difference between linear one and 3D nanomachines for target cell-surface recognition and computing (Figure 3b). As these DNA nanomachines were stable within 6 h in 10% fetal bovine serum (Figure 3a), they were then used to test the responses to CEM (targeted cell) and Ramos (control cell, Figures S6 and S7). In order to adequately interacting with cell surface, nanomachines were initially incubated at 4 °C for 1 h, final signals were obtained after further different incubation times, ranging from 1 h, 2 to 4 h. Interestingly, the stronger and faster fluorescence intensity in the DNA-logic gate TP group was observed for "ON" signal (Figure 3c). We speculated that nanomachines completed the recognition and computing processes within the first 1 h; meanwhile, their cellular internalization became the main factor for signal obtain, which provide a strategy for constructing structural molecular machines when taking final signal into consideration. Importantly, the improvement of diagnosis accuracy can be implemented by employing dual or even multiple molecular recognition, thus providing a path for construction of advanced and powerful nanomachines.

To study the specificity and selectivity of our 3D DNA-logic-gate TP for cell-surface computing, it was tested on both CEM (target group) and Ramos (control group) cells. After a reporter toe was loaded onto the top face of the DNA-logic gate TP scaffold to assemble a prismatic nanostructure, different aptamer-based recognition toes were loaded on its bottom face, ultimately forming such logic nanostructures as sgc8c-F/S/R-TP, sgc4f-F/S/R-TP, sgc8c-sgc4f-F/S/R-TP, sgc8c/cS-F/S/R-TP, sgc4f/cF-F/S/R-TP and sgc8c/cS- sgc4f/cF-F/S/R-TP (the intact DNA-logic gate TP). These DNA nanostructures were respectively incubated with CEM and Ramos cells to study the effects of different functional segments. Then, flow cytometry was employed to analyze the effects of logic operations on the two cell types for 1 h (Figure S8), 2 h (Figure S9), and 4 h (Figure S10). Among all groups shown in Figure 4a, the fluorescence intensity of sgc8c/cS-sgc4f/cF-F/S/R-TP incubated

with CEM cells was highest. This result demonstrated that the intact DNA-logic gate TP could perform “recognition-then-computing” operation completely and that the signal “ON” feedback could be obtained. For the different times tested, a divergence in selectivity between control Ramos and CEM target groups was gradually displayed. Confocal laser scanning microscopy imaging of the DNA-logic gate TP at different times was in agreement with the flow cytometry results (Figure 4b).

Heterogeneity is a characteristic of cancer cells, particularly protein receptors on the cell surface. Single recognition molecules cannot identify all clinical samples from various patients, even those with the same cancer type. Therefore, it follows that a bispecific “recognition-then-computing”[19] nanomachine would be especially desirable in the context of diagnostics/therapeutics. Indeed, our 3D DNA-logic gate TP meets this requirement based on its ability to rapidly distinguish biomarkers of interest in living cells in situ. This strategy is also applicable for RNA nanostructures and large DNA architectures.[9a] Additionally, combination of the molecular proximity effect[20] and DNA nanotechnology[16a] for engineering nanodevices is largely employed in the field of biomedicine, and our small and simple DNA nanomachine is more easily designed, economical, and powerful than other massive DNA nanostructures.

As proof-of-concept, we designed and engineered an aptamer-based 3D DNA-logic gate TP nanomachine. This nanomachine is proposed to perform Boolean logic operations on the membrane surfaces of cancer cells, in particular the AND operation. Not only could this nanomachine perform cell surface-based logic operations, but it could also be easily internalized, indicating its theranostic potential. Different from linear dsDNA-based circuits, this 3D DNA nanomachine easily incorporated all logic units into one triangular scaffold able to report “ON” when the specific cell type is presented, thus improving the accuracy of cell identification. Otherwise, the reporter toe is signal “OFF” when the target cell is absent, thus bringing a smart diagnostic tool to the forefront of personalized medicine and biomedical research.

Supplementary Material

Refer to Web version on PubMed Central for supplementary material.

ACKNOWLEDGMENTS

This work is supported by NSFC grants (NSFC 21521063, NSFC 21675043), by NIH R35 GM 127130 and NSF 1645215.

REFERENCES

(1) (a). Dejana E Nat. Rev. Mol. Cell Biol 2004, 5, 261–270. [PubMed: 15071551] (b)Kania A; Klein R Nat. Rev. Mol. Cell Biol 2016, 17, 240–256. [PubMed: 26790531]

(2) (a). Nishino M; Ramaiya NH; Hatabu H; Hodi FS Nat. Rev. Clin. Oncol 2017, 14, 655–668. [PubMed: 28653677] (b)Zhang L; Wan S; Jiang Y; Wang Y; Fu T; Liu Q; Cao Z; Qiu L; Tan WJ Am. Chem. Soc 2017, 139, 2532–2540.

(3). Erbas-Cakmak S; Leigh DA; McTernan CT; Nussbaumer AL Chem. Rev 2015, 115, 10081–10206. [PubMed: 26346838]

(4) (a). Rudchenko M; Taylor S; Pallavi P; Dechkovskaia A; Khan S; Butler VP, Jr.; Rudchenko S; Stojanovic MN Nat. Nanotechnol 2013, 8, 580–586. [PubMed: 23892986] (b)You MX; Zhu G; Chen T; Donovan MJ; Tan WJ Am. Chem. Soc 2015, 137, 667–674.

(5). Zhu GZ; Zheng J; Song E; Donovan M; Zhang K; Liu C; Tan W Proc. Natl. Acad. Sci. U. S. A 2013, 110, 7998–8003. [PubMed: 23630258]

(6). Han D; Wu C; You M; Zhang T; Wan S; Chen T; Qiu L; Zheng Z; Liang H; Tan W Nat. Chem 2015, 7, 835–841. [PubMed: 26391084]

(7) (a). Qu X; Zhu D; Yao G; Su S; Chao J; Liu H; Zuo X; Wang L; Shi J; Wang L; Huang W; Pei H; Fan C Angew. Chem., Int. Ed 2017, 56, 1855–1858.(b)Zhang S; Wang K; Huang C; Li Z; Sun T; Han DM Nanoscale 2016, 8, 15681–15688. [PubMed: 27524500]

(8). Morris W; Briley WE; Auyeung E; Cabezas MD; Mirkin CA J. Am. Chem. Soc 2014, 136, 7261–7264. [PubMed: 24818877]

(9) (a). Douglas SM; Bachelet I; Church GM Science 2012, 335, 831–834. [PubMed: 22344439] (b)He KY; Li Y; Xiang B; Zhao P; Hu Y; Huang Y; Li W; Nie Z; Yao S Chem. Sci 2015, 6, 3556–3564. [PubMed: 30154999]

(10). Han D; Qi X; Myhrvold C; Wang B; Dai M; Jiang S; Bates M; Liu Y; An B; Zhang F; Yan H; Yin P Science 2017, 358, eaao2648.

(11). You M; Lyu Y; Han D; Qiu L; Liu Q; Chen T; Wu SC; Peng L; Zhang L; Bao G; Tan W Nat. Nanotechnol 2017, 12, 453–459. [PubMed: 28319616]

(12). Meng HM; Liu H; Kuai H; Peng R; Mo L; Zhang XB Chem. Soc. Rev 2016, 45, 2583–2602. [PubMed: 26954935]

(13) (a). Shangguan D; Li Y; Tang Z; Cao ZC; Chen HW; Mallikaratchy P; Sefah K; Yang CJ; Tan W Proc. Natl. Acad. Sci. U. S. A 2006, 103, 11838–11843. [PubMed: 16873550] (b)Liang C; Guo B; Wu H; Shao N; Li D; Liu J; Dang L; Wang C; Li H; Li S; Lau WK; Cao Y; Yang Z; Lu C; He X; Au DW; Pan X; Zhang BT; Lu C; Zhang H; Yue K; Qian A; Shang P; Xu J; Xiao L; Bian Z; Tan W; Liang Z; He F; Zhang L; Lu A; Zhang G Nat. Med 2015, 21, 288–294. [PubMed: 25665179]

(14). You MX; Peng L; Shao N; Zhang L; Qiu L; Cui C; Tan WJ Am. Chem. Soc 2014, 136, 1256–1259.

(15). Conway JW; McLaughlin CK; Castor KJ; Sleiman H Chem. Commun 2013, 49, 1172–1174.

(16) (a). Chen YJ; Groves B; Muscat RA; Seelig G Nat. Nanotechnol 2015, 10, 748–760. [PubMed: 26329111] (b)Blanco E; Shen H; Ferrari M Nat. Biotechnol 2015, 33, 941–951. [PubMed: 26348965]

(17) (a). Conway JW; Madwar C; Edwardson TG; McLaughlin CK; Fahkoury J; Lennox RB; Sleiman HF J. Am. Chem. Soc 2014, 136, 12987–12997. [PubMed: 25140890] (b)Peng R; Wang H; Lyu Y; Xu L; Liu H; Kuai H; Liu Q; Tan WJ Am. Chem. Soc 2017, 139, 12410–12413.

(18). Ren K; Liu Y; Wu J; Zhang Y; Zhu J; Yang M; Ju H Nat. Commun 2016, 7, 13580. [PubMed: 27882923]

(19). Cui C; Zhang H; Wang R; Cansiz S; Pan X; Wan S; Hou W; Li L; Chen M; Liu Y; Chen X; Liu Q; Tan W Angew. Chem., Int. Ed 2017, 56, 11954–11957.

(20) (a). Shrestha P; Jonchhe S; Emura T; Hidaka K; Endo M; Sugiyama H; Mao H Nat. Nanotechnol 2017, 12, 582–588. [PubMed: 28346457] (b)Küchler A; Yoshimoto M; Luginbühl S; Mavelli F; Walde P Nat. Nanotechnol 2016, 11, 409–420. [PubMed: 27146955]

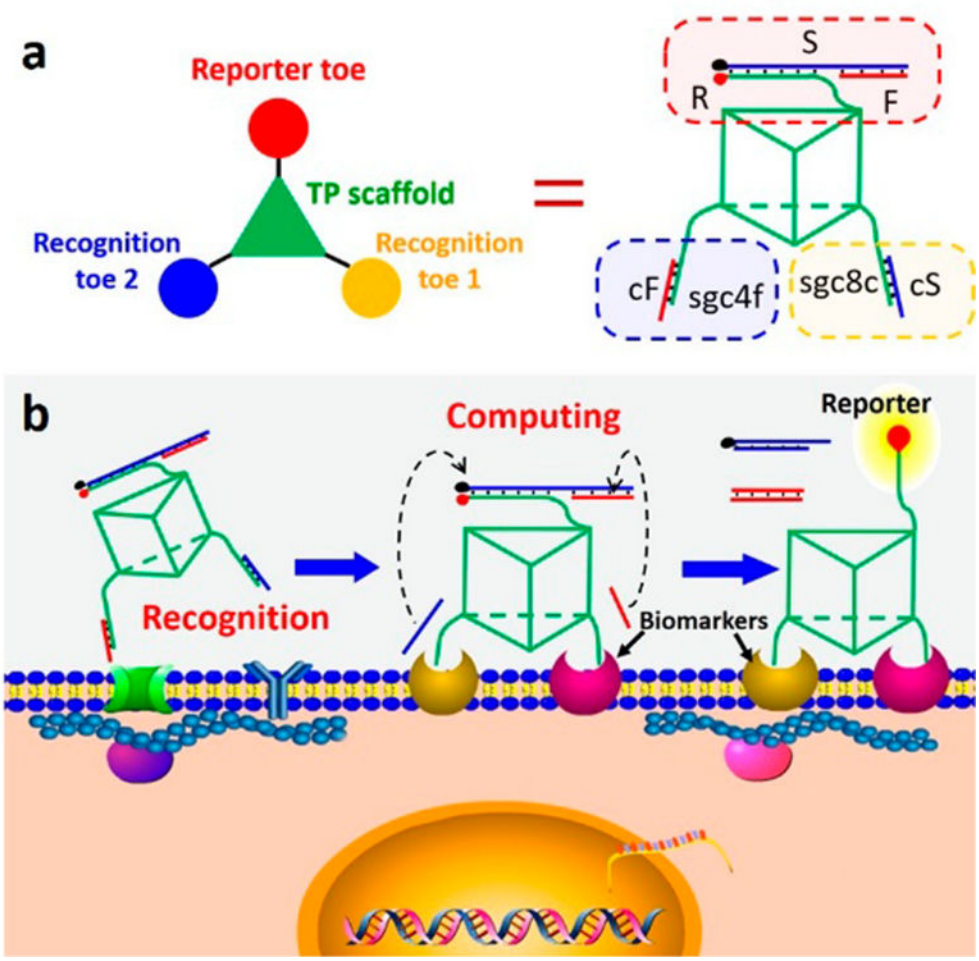

Figure 1.

Working principles of DNA engineered nanomachine. (a) Structural diagram of DNA-logic gate TP nanomachine, which contains reporter toe, recognition toe 1, recognition toe 2 and DNA TP scaffold. Strand cS is completely complementary to strand S and a piece of sgc8c, whereas strand cF is completely complementary to strand F and a piece of sgc4f. (b) Scheme of aptamer-based 3D DNA nanomachine for targeted cell surface computing. Two aptamers recognize and bind to their membrane biomarkers, thus releasing cS and cF from respective recognition toes. Driven by DNA strand displacement reactions, the fluorescence signal in reporter toe switches to “ON” from its original quenched (OFF) state.

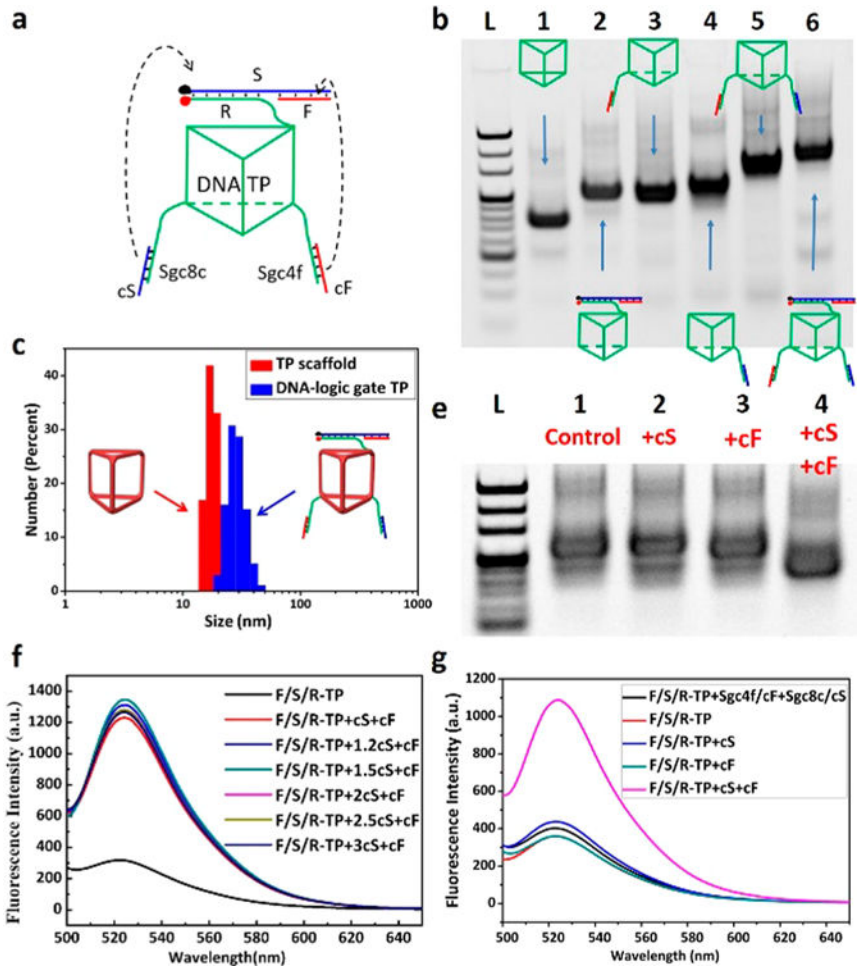

Figure 2.

Self-assembly and dynamic logic operation of 3D DNA- logic gate nanomachine in buffer solution. (a) Dynamic operation of the DNA-logic gate nanomachine. (b) Native-PAGE results confirmed the stepwise assembly of the DNA-logic gate TP. Lane 1: DNA TP scaffold. Lane 2: F/S/R-TP. Lane 3: sgc8c/cS-TP. Lane 4: sgc4f/cF-TP. Lane 5: sgc8c/cS-sgc4f/cF-TP. Lane 6: F/S/R-sgc8c/ cS-sgc4f/cF-TP (DNA-logic gate TP). (c) Determination of the size of 500 nM TP scaffold (red) and DNA-logic gate TP (blue) by DLS. (e) Native-PAGE analysis of the dynamic behavior of the DNA-logic gate TP. Lane 1: DNA-logic gate TP. Lane 2−3: previous sample adding either cS or cF, respectively. Lane 4: DNA-logic gate TP, adding both cS and cF. Lane L: DNA ladder. (f) Ratio optimization of cS and cF. Fluorescence intensity was recorded for FAM-R and BHQ 1-S loaded DNA TP. (g) Fluorescence change of DNA-logic gate TP in response to DNA strand displacement.

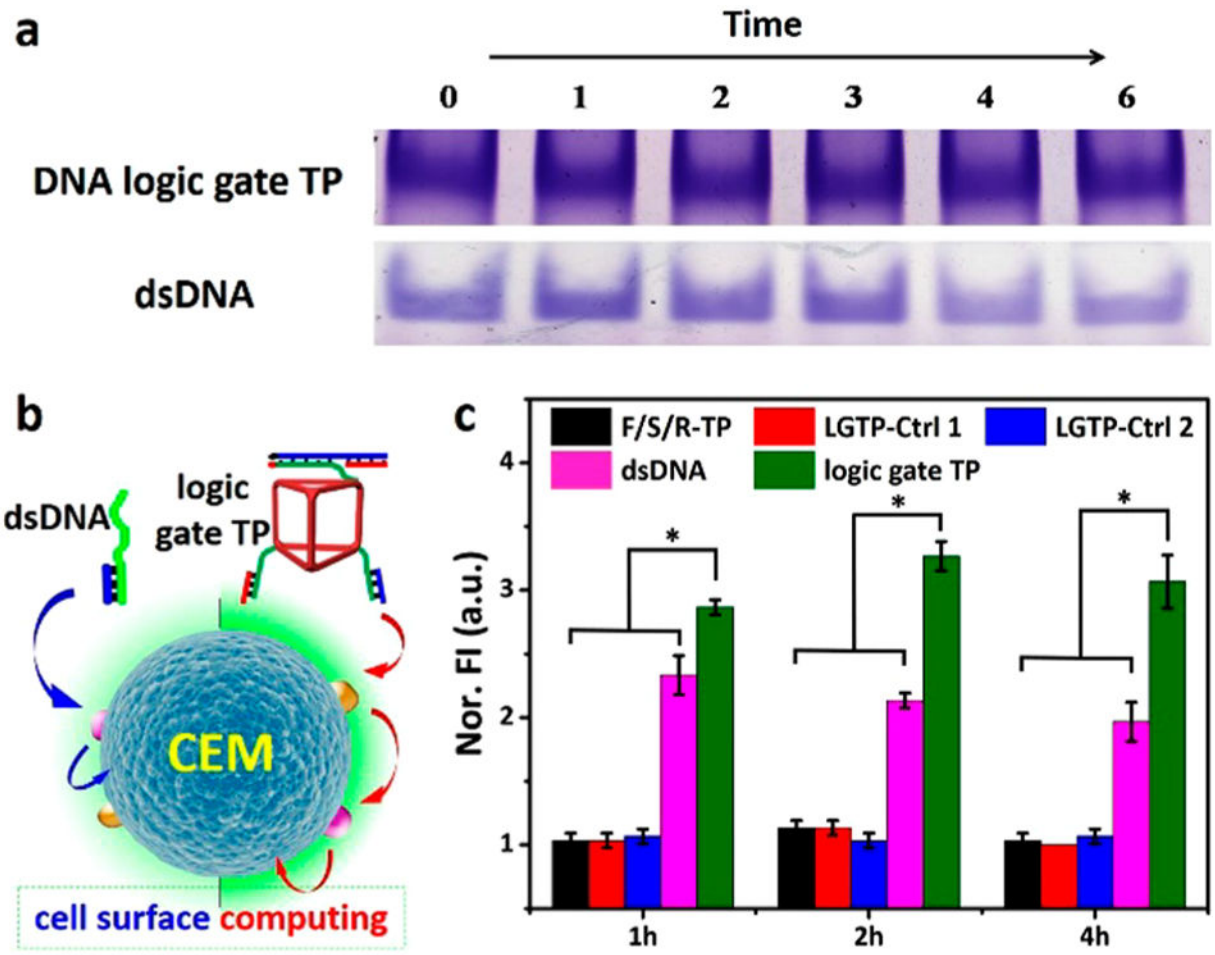

Figure 3.

Difference between linear dsDNA and the 3D DNA-logic gate TP for target cell surface computing. (a) Degradation analysis between 3D DNA-logic gate TP and double stranded DNA. Native polyacrylamide gel analysis of FBS (10% v/v) degradation assay products for DNA-logic gate TP and dsDNA within 6 h. (b) Schematic illustration representing the logic operations of respective dsDNA (left) and DNA-logic gate TP (right) on the target cell surface. (c) The fluorescence intensity of DNA-logic gate TP comparing with dsDNA and control groups (F/S/R-TP, LGTP-Ctrl 1 and LGTP-Ctrl 1) shows the difference between linear double- strand DNA machine and 3D logic gate nanomachine. *P* values were calculated by Newman−Keuls Multiple Comparison Test, $*P < 0.05$. The fluorescence values and their error bars were calculated from three experiments.

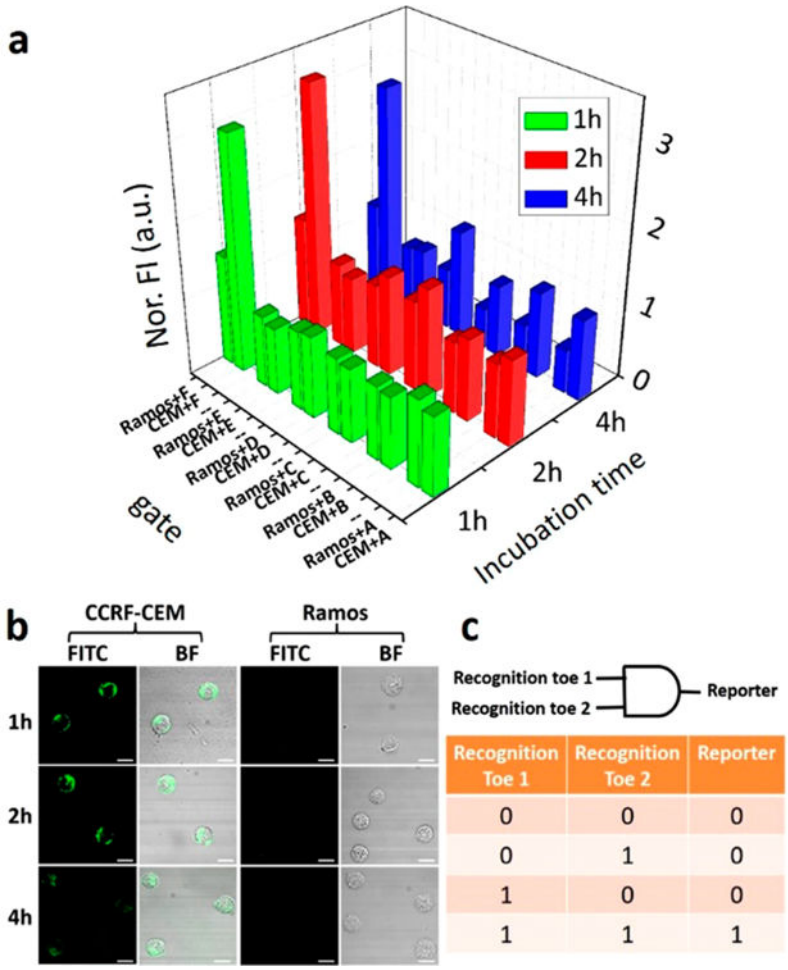

Recognition Toe 1	Recognition Toe 2	Reporter
0	0	0
0	1	0
1	0	0
1	1	1

Figure 4.

3D DNA-logic gate nanomachine for cell-surface recognition and computing. (a) Flow cytometry reporting signals of different DNA TP-based nanostructures for both CEM and Ramos cells during incubation times of 1 h, 2 and 4 h; A: sgc8c-F/S/R-TP, B: sgc4f-F/S/R-TP, C: sgc8c-sgc4f-F/S/R-TP, D: sgc8c/cS-F/S/R-TP, E: sgc4f/cF-F/S/R-TP, F: sgc8c/cS-sgc4f/cF-F/S/R-TP (DNA-logic gate TP). Only the intact logic gate TP can accomplish the steps of bispecific biomarker recognition, DNA strand displacement reaction- based computing and effective fluorescent reporting. (b) Confocal laser scanning microscopy images of CEM and Ramos cells interacting with the 3D DNA-logic gate nanomachine for 1 h, 2 and 4 h. Scale bar = 10 μm. (c) Truth table of DNA logic-gate nanomachine.